Entropy Generation on Pulsatile Hydromagnetic Flow of Jeffrey Nanofluid in a Porous Channel with Brownian Motion, Thermophoresis, and Heat Source/Sink Using Cattaneo-Christov Heat Flux

T Thamizharasan & A Subramanyam Reddy*

Department of Mathematics, School of Advanced Sciences, Vellore Institute of Technology, Vellore-632 014, Tamil Nadu, India

In this work, the entropy generation on MHD pulsatile flow of Jeffrey nanofluid in a porous channel with Cattaneo-Christov theory is investigated. Buongiorno nanofluid model is utilized to see the impact of thermophoresis and Brownian motion. The consequences of thermal radiation, heat source/sink, viscous dissipation, and Ohmic heating are considered. The governing equations are transformed to a system of ordinary differential equations by applying the perturbation procedure then numerically tackled with fourth-order Runge-Kutta scheme aided by shooting technique. The influences of different emerging parameters and variables on velocity, temperature, nanoparticles concentration, entropy generation, and Bejan number are presented graphically. The influence of emerging parameters on heat and mass transfer rates are prearranged in table. The temperature of nanofluid increases with an enhancement in Eckert number, thermophoretic, and Brownian movements, whereas it decelerates for the rising values of cross flow Reynolds number. The concentration of nanoparticles diminishes with an increment in the Lewis number, chemical reaction parameter, and Brownian motion parameter whereas it improves with a rise in thermophoresis parameter. The entropy generation is an increasing function of Eckert number and radiation parameter. Further, the Bejan number is enhanced for increasing the values of Hartmann number.

Keywords: Jeffrey nanofluid; Pulsatile flow; Entropy generation; Cattaneo-Christov heat flux; Brownian motion; Thermophoresis

1 Introduction

Over the decades, significant studies have been conducted to explore the role of pulsatory flow in a channel or pipe due to its importance in biological and industrial applications. These include electronic cooling, drying technology, packed bed heat exchangers, geothermal systems, catalytic reactors, and so on[1–6]. Wang *et al.*[7] numerically studied the oscillatory flow of blood and heat transfer via small vessels with radiative heat and Ohmic heating consequences by executing the finite difference scheme. Ali *et al.*[8] inspected the Casson fluid flow with oscillation through a permeable channel. Sadeghi *et al.*[9] investigated the pulsatory non-Newtonian blood flow through an flexible artery in the existence of a magnetic field influence. Selvi *et al.*[10] utilized the method of integral transform to study the influence of radiative heat and electromagnetic field on pulsatory non-Newtonian flow of blood through a tapered stenosed artery with a permeable medium. Shit *et al.*[11]

deliberated the oscillating blood flow via permeable overlapping confined artery with viscous dissipation and a magnetic field impacts. Recently, Govindarajulu & Reddy[12] scrutinized the oscillating hybrid third grade nanofluid flow through a permeable channel in the presence of viscous dissipation and a magnetic field.

Non-Newtonian fluids have been exploring different applications in various fields. Non-Newtonian fluids like toothpaste, blood, ketchup, paint, and many others are used extensively in our daily lives. The three types of non-Newtonian fluids are integral, rate, and differential. Specifically, Jeffrey model deals with retardation time and the ratio of relaxation time to retardation time in Jeffrey fluids, which constitute a sub-class of rate type fluids[13–17]. Khan *et al.*[18] inspected the hydromagnetic stagnation Jeffrey nanoliquid flow over an extending sheet under the influences of Brownian movements and thermophoretic by employing the Cattaneo Christov theory. Saif *et al.*[19] presented the heat source and sink consequences on Jeffrey nanoliquid flow passing on a extendable curved sheet. Hayat *et al.*[20] analytically

*Corresponding authors:
(Email: anala.subramanyamreddy@gmail.com)

presented the flow of Jeffrey fluid passing a spinning disk by implementing the homotopy analysis method. Chu et al.[21] calculated the third grade fluid flow on a stretchable plane in the existence of viscous dissipation and chemical reaction consequences with help of Buongiorno model. Khan et al.[22] utilized the homotopy analysis method to examine the hydromagnetic stagnation flow of Jeffrey nanoliquid on a plane. Hussain et al.[23] explained the heat flux of Cattaneo-Christov in Jeffrey fluid flow passing an extending cylinder in the existence of thermal relaxation and chemical reaction.

Recently, many researchers have become interested in studying nanotechnology due to its widespread applications. Nanofluid is a combination of common fluids and nanoparticles with average sizes ranging from 1 to 100nm[24–30]. Dogonchi and Ganji[31] investigated the heat transfer and hydromagnetic nanofluid flow between two parallel plates with radiative heat effects by applying the Cattaneo-Christov theory. Abbas et al.[32] discussed the nanofluid (Cu-H_2O) in a square cavity with two obstacles in the presence of magnetic field by implementing a Galerkin finite element Method. Hayat et al.[33] scrutinized the magnetic field and heat generation impacts of second-grade nanofluid flow over a stretchable Riga wall with Cattaneo-Christov model. Dogonchi et al.[34] explored the heat transfer and nanoliquid flow between two parallel disks with the impressions of thermal relaxation and radiative heat. Hamid et al.[35] used the finite difference technique to study the hydromagnetic flow of Williamson nanoliquid between a permeable channel along with the Brownian movement and thermophoretic consequences.

Entropy is the quantity of energy produced in a thermal system by irreversible processes. It has been observed that such thermal energy is incapable of being put to any useful use. As a result, lowering entropy formation is advantageous for improving the thermal system's performance[36–40]. Hayat et al.[41] scrutinized the entropy production with viscous dissipation, Ohmic heating, radiative heat effects on hydromagnetic Jeffrey nanoliquid flow on an extendable sheet. Almakki et al.[42] presented the MHD Jeffrey nanoliquid flow in a permeable stretching sheet with entropy generation. Entropy generation on Jeffrey nanoliquid flow passes a variable thickened surface with Ohmic heating and nonlinear radiative heat flux is explored by Javed et al.[43]. Pal et al.[44] numerically scrutinized the hydromagnetic Jeffrey

nanoliquids flow on a linear stretchy surface in the presence of radiative heat by using the Runge-Kutta-Fehlberg method. Rehman et al.[45] investigated the entropy generation on the flow of Jeffrey nanofluid by a extendable sheet with the help of the Buongiorno model.

The major purpose of this study is to analyze the influence of the Cattaneo-Christov heat flux model on pulsatile Jeffrey nanofluid flow through a porous channel with entropy generation. Buongiorno nanofluid model is considered to see Brownian movements and thermophoretic impacts. The impression of Ohmic heating, radiative heat, and heat source/sink are considered. The governing equations are transformed to a system of ordinary differential equations by applying the perturbation procedure then numerically tackled with fourth-order Runge-Kutta scheme aided by shooting technique. This work is useful for biofluidic engineering, blood cancer treatment, nano-drug delivery, pharmaceutical process, chemical engineering, and biomedical aspects. The influence of various physical parameters and variables on velocity, temperature, nanoparticles concentration, entropy generation, and Bejan number are presented graphically. The heat and mass transfer rates are tabulated for different values of emerging parameters and discussed in detail.

2 Formulation of the problem

In this analysis, we consider pulsating electrically conducting laminar and incompressible flow of Jeffrey nanoliquid in a porous channel with the Cattaneo-Christov model. Chemical reaction, radiative heat, viscous dissipation, Ohmic heating, and heat source/sink are considered. The flow geometry of the model is presented in Fig. 1 shows
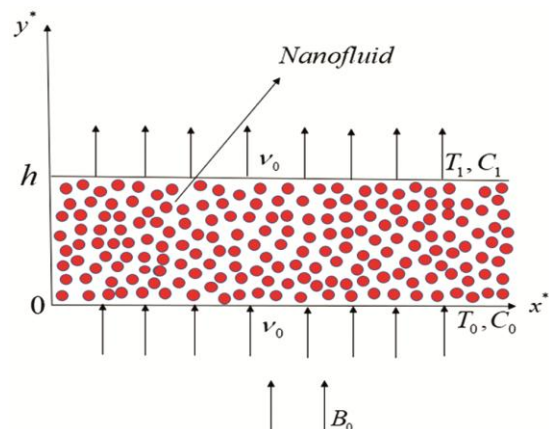

Fig. 1 — Coordinate system of geometry.

that the bottom wall is parallel to the x^*-axis and y^*-axis runs perpendicular to the walls, h indicates hight between the plates. A magnetic field of intensity B_0 is applying normal to the flow direction. $T_1(>T_0)$ and T_0 are the temperatures of the top and bottom walls and $C_1(>C_0)$ and C_0 are the concentration of the nanoparticles of the top and bottom walls respectively.

Assume that the pulsating flow is induced by the pressure gradient of the form [4, 5]

$$-\frac{1}{\rho_f}\frac{\partial P^*}{\partial x^*} = A(1+\varepsilon e^{i\omega t^*}), \qquad \qquad \ldots(1)$$

here t^* is dimensional time, ω is frequency, $\varepsilon(<<1)$ is a positive quantity, A is constant, P^* is the dimensional pressure. By these assumptions the governing equations are,

$$\rho_f\left(\frac{\partial u^*}{\partial t^*} + v_0\frac{\partial u^*}{\partial y^*}\right) = -\frac{\partial P^*}{\partial x^*} + \frac{\mu_f}{1+\lambda_1}\frac{\partial^2 u^*}{\partial y^{*2}}$$

$$+\frac{\lambda_2\mu_f}{1+\lambda_1}\frac{\partial^3 u^*}{\partial t^*\partial y^{*2}} - \sigma_f B_0^2 u^*, \qquad \ldots(2)$$

$$\frac{\partial T^*}{\partial t^*} + v_0\frac{\partial T^*}{\partial y^*} + \alpha\left(\frac{\partial^2 T^*}{\partial t^{*2}} + 2v_0\frac{\partial^2 T^*}{\partial t^*\partial y^*}\right.$$

$$\left.+v_0^2\frac{\partial^2 T^*}{\partial y^{*2}}\right) = \frac{K_f}{(\rho C_p)_f}\frac{\partial^2 T^*}{\partial y^{*2}}$$

$$+\frac{1}{(\rho C_p)_f}\frac{\mu_{nf}}{1+\lambda_1}\left(\frac{\partial u^*}{\partial y^*}\right)^2 - \frac{1}{(\rho C_p)_f}\frac{\partial q_r}{\partial y^*}$$

$$+\frac{\sigma_f B_0^2}{(\rho C_p)_f}u^{*2} + \frac{Q_0}{(\rho C_p)_f}\left(T^* - T_0\right)$$

$$+\tau\left[D_B\left(\frac{\partial C^*}{\partial y^*}\frac{\partial T^*}{\partial y^*}\right) + \frac{D_T}{T_m}\left(\frac{\partial T^*}{\partial y^*}\right)^2\right], \qquad \ldots(3)$$

$$\frac{\partial C^*}{\partial t^*} + v_0\frac{\partial C^*}{\partial y^*} = D_B\frac{\partial^2 C^*}{\partial y^{*2}}$$

$$+\frac{D_T}{T_m}\frac{\partial^2 T^*}{\partial y^{*2}} - k_1 C^*. \qquad \ldots(4)$$

Where u^* is component of dimensional velocity in x^*- direction, μ_f is dynamic viscosity of the fluid,

ρ_f is density of fluid, λ_1 and λ_2 material parameters of Jeffrey fluid, σ_f is the electrical conductivity of the fluid, K_f is thermal conductivity of fluid, q_r is radiative heat flux, $\tau = (\rho C_p)_p / (\rho C_p)_f$, $(\rho C_p)_f$ is heat capacitance of fluid, $(\rho C_p)_p$ is the effective heat capacity of the nanoparticles, T^*, C^* are the temperature and concentration , K_1 is the rate of first order chemical reaction, D_B is Brownian diffusion coefficient, D_T is thermophoresis diffusion coefficient, and T_m is mean temperature.

The appropriate boundary conditions are

At $y^* = 0 \Rightarrow u^* = 0, T^* = T_0, C^* = C_0,$ $\qquad \ldots(5)$

At $y^* = h \Rightarrow u^* = 0, T^* = T_1, C^* = C_1.$ $\qquad \ldots(6)$

By applying the Rosseland estimation for q_r and following [24, 25], Eq. (3) becomes

$$\frac{\partial T^*}{\partial t^*} + \alpha\left(\frac{\partial^2 T^*}{\partial t^{*2}} + 2v_0\frac{\partial^2 T^*}{\partial t^*\partial y^*} + v_0^2\frac{\partial^2 T^*}{\partial y^{*2}}\right)$$

$$+v_0\frac{\partial T^*}{\partial y^*} = \frac{K_f}{(\rho C_p)_f}\frac{\partial^2 T^*}{\partial y^{*2}}$$

$$+\frac{1}{(\rho C_p)_f}\frac{\mu_{nf}}{1+\lambda_1}\left(\frac{\partial u^*}{\partial y^*}\right)^2$$

$$+\frac{1}{(\rho C_p)_f}\frac{16\sigma^* T_0^3}{3\chi}\frac{\partial^2 T^*}{\partial y^{*2}}$$

$$+\frac{\sigma_f B_0^2}{(\rho C_p)_f}u^{*2} + \frac{Q_0}{(\rho C_p)_f}\left(T^* - T_0\right)$$

$$+\tau\left[D_B\left(\frac{\partial C^*}{\partial y^*}\frac{\partial T^*}{\partial y^*}\right) + \frac{D_T}{T_m}\left(\frac{\partial T^*}{\partial y^*}\right)^2\right], \qquad \ldots(7)$$

here, σ^* is the Stephen-Boltzmann constant and χ is the Rosseland mean absorption coefficient.

Now, by following the non-dimensional parameters and variables,

$$P = \frac{P^*}{A\rho_f h}, \; u = \frac{u^*\omega}{A}, \; x = \frac{x^*}{h}, \; y = \frac{y^*}{h},$$

$$t = t^*\omega, \; \theta = \frac{T^* - T_0}{T_1 - T_0}, \; \phi = \frac{C^* - C_0}{C_1 - C_0}. \qquad \ldots (8)$$

Eqs. (1), (2), (7), and (4) become

$$-\frac{\partial P}{\partial x} = 1 + \varepsilon e^{it}, \qquad \ldots (9)$$

$$H^2 \frac{\partial u}{\partial t} + R \frac{\partial u}{\partial y} = -H^2 \frac{\partial P}{\partial x}$$

$$+ \frac{1}{1+\lambda_1}\frac{\partial^2 u}{\partial y^2} + \frac{\lambda}{1+\lambda_1}\frac{\partial^3 u}{\partial t \partial y^2} - M^2 u, \qquad \ldots (10)$$

$$H^2 \frac{\partial \theta}{\partial t} + R \frac{\partial \theta}{\partial y} + \delta\left(\frac{\partial^2 \theta}{\partial t^2} H^2 + 2R\frac{\partial^2\theta}{\partial t \partial y} \right.$$

$$\left. + \frac{R^2}{H^2}\frac{\partial^2\theta}{\partial y^2} \right) = \frac{1}{Pr}\left(1 + \frac{4}{3}Rd\right)\frac{\partial^2\theta}{\partial y^2}$$

$$+ \frac{Ec}{1+\lambda_1}\left(\frac{\partial u}{\partial y}\right)^2 + M^2 Ec u^2 + Nb\frac{\partial\theta}{\partial y}\frac{\partial\phi}{\partial y}$$

$$+ Nt\left(\frac{\partial\theta}{\partial y}\right)^2 + Q\theta, \qquad \ldots (11)$$

$$Le\,Pr\,H^2 \frac{\partial\phi}{\partial t} + R\,Pr\,Le\frac{\partial\phi}{\partial y} = \frac{\partial^2\phi}{\partial y^2}$$

$$+ \frac{Nt}{Nb}\frac{\partial^2\theta}{\partial y^2} - \gamma Le\,Pr\,\phi - K_1 Le\,Pr. \qquad \ldots (12)$$

Where $H = h\sqrt{\dfrac{\omega}{v_f}}$ is the frequency parameter,

$Pr = \dfrac{(\rho C_p)_f v_f}{K_f}$ is the Prandtl number, $M = B_0 h\sqrt{\dfrac{\sigma_f}{\mu_f}}$ is

the Hartmann number, $Rd = \dfrac{4\sigma^* T_1^3}{K_f \chi}$ is the radiation

parameter, $R = \dfrac{v_0 h}{v_f}$ is cross flow Reynolds number,

$\lambda = \lambda_2\omega$ is the dimensionless material parameter,

$Ec = \dfrac{A^2}{\omega^2 (C_p)_f (T_1 - T_0)}$ is the Eckert number,

$\delta = \omega\alpha$ is the thermal relaxation time parameter,

$Q = \dfrac{Q_0 h^2}{(\rho C_p)_f v_f}$ is the heat source/sink parameter,

$Nt = \dfrac{\tau D_T (T_1 - T_0)}{T_m v_f}$ is the thermophoresis parameter,

$Le = \dfrac{k_f}{(\rho C_p)_f D_B}$ is Lewis number, $Nb = \dfrac{\tau D_B (C_1 - C_0)}{v_f}$

is the Brownian motion parameter, $\gamma = \dfrac{k_1 h^2}{v_f}$ is

chemical reaction parameter, and $K_1 = \dfrac{k_1 C_0 h^2}{v_f (C_1 - C_0)}$.

The Corresponding boundary conditions are

$$u(0) = 0, \; \theta(0) = 0, \; \phi(0) = 0, \qquad \ldots (13)$$
$$u(1) = 0, \; \theta(1) = 1, \; \phi(1) = 1. \qquad \ldots (14)$$

3 Solution of the problem

On account of Eq. (9), the velocity, temperature, and concentration can be conveyed as follows:

$$u = u_0(y) + \varepsilon u_1(y)e^{it} \qquad \ldots (15)$$

$$\theta = \theta_0(y) + \varepsilon\theta_1(y)e^{it} \qquad \ldots (16)$$

$$\phi = \phi_0(y) + \varepsilon\phi_1(y)e^{it} \qquad \ldots (17)$$

Using Eqs. (9), (15), (16), and (17) in Eqs. (10)-(12) and then likening the corresponding coefficient of different powers of ε, we get

$$\left(\frac{1}{1+\lambda_1}\right)u_0'' - Ru_0' - M^2 u_0 + H^2 = 0, \qquad \ldots (18)$$

$$\left(\frac{1}{1+\lambda_1} + \frac{\lambda i}{1+\lambda_1}\right)u_1'' - Ru_1'$$

$$-\left[M^2 + iH^2\right]u_1 + H^2 = 0 \qquad \ldots (19)$$

$$\left(\left(1+\frac{4}{3}Rd\right)\frac{1}{\Pr}-\delta\frac{R^2}{H^2}\right)\theta_0''-R\theta_0'$$

$$+Q\theta_0+Nb\phi_0'\theta_0'+Nt\left(\theta_0'\right)^2$$

$$+\frac{Ec}{1+\lambda_1}\left(u_0'\right)^2+M^2Ecu_0^2=0, \qquad\qquad \dots (20)$$

$$\left(\left(1+\frac{4}{3}Rd\right)\frac{1}{\Pr}-\delta\frac{R^2}{H^2}\right)\theta_1''-R\theta_1'$$

$$+Q\theta_1+Nb\left(\theta_0'\phi_1'+\theta_1'\phi_0'\right)-iH^2\theta_1$$

$$+\frac{Ec}{1+\lambda_1}2u_0'u_1'+2M^2Ecu_0u_1$$

$$+2Nt\theta_0'\theta_1'-\delta H^2i^2\theta_1-2\delta Ri\theta_1'=0, \qquad \dots (21)$$

$$\phi_0''-\gamma Le\Pr\phi_0+\left(\frac{Nt}{Nb}\right)\theta_0''$$

$$-Le\Pr R\phi_0'-K_1Le\Pr=0, \qquad\qquad \dots (22)$$

$$\phi_1''-Le\Pr\left(iH^2+\gamma\right)\phi_1$$

$$+\left(\frac{Nt}{Nb}\right)\theta_1''-Le\Pr R\phi_1'=0. \qquad\qquad \dots (23)$$

The appropriate boundary conditions are

$$\left.\begin{array}{l}u_0(0)=0,\ \theta_0(0)=0,\ \phi_0(0)=0\\u_1(0)=0,\ \theta_1(0)=0,\ \phi_1(0)=0\end{array}\right\}, \qquad \dots (24)$$

$$\left.\begin{array}{l}u_0(1)=0,\ \theta_0(1)=1,\ \phi_0(1)=1\\u_1(1)=0,\ \theta_1(1)=0,\ \phi_1(1)=0\end{array}\right\}. \qquad \dots (25)$$

Now, the non-dimensional heat transfer rate (Nusselt number Nu) and mass transfer rate
(Sherwood number Sh) at the walls is given as [5, 17, 37],

$$Nu=\left(1+\frac{4}{3}Rd\right)\left(\frac{d\theta_0}{dy}+\varepsilon e^{it}\frac{d\theta_1}{dy}\right)_{y=0,1}\ \text{and}$$

$$Sh=\left(\frac{d\phi_0}{dy}+\varepsilon e^{it}\frac{d\phi_1}{dy}\right)_{y=0,1} \qquad \dots (26)$$

Equations [18]-[23] are solved by utilizing the shooting technique with the Runge-Kutta fourth-order

procedure with boundary conditions [24] and [25]. The step size $0.001\left(\Delta y=0.001\right).1\times10^{-10}$ correctness is fixed for the convergence criteria.

3.1 Entropy generation analysis

The dimensional form of entropy generation of the current work is given as [37-39]

$$SG=\frac{K_f}{T_0^2}\left(1+\frac{16\sigma^*T_0^3}{3K_f\chi}\right)\left(\frac{\partial T^*}{\partial y^*}\right)^2$$

$$+\frac{\mu_f}{\left(1+\lambda_1\right)T_0}\left(\frac{\partial u^*}{\partial y^*}\right)^2+\frac{\sigma B_0^2}{T_0}u^{*2}$$

$$+\frac{R_1D}{C_0}\left(\frac{\partial C^*}{\partial y^*}\right)^2+\frac{R_1D}{T_0}\left(\frac{\partial T^*}{\partial y^*}\right)\left(\frac{\partial C^*}{\partial y^*}\right). \qquad \dots (27)$$

The non-dimensional form of entropy generation is

$$NG=\left(1+\frac{4Rd}{3}\right)\left(\theta'\right)^2+\frac{Ec\Pr}{\left(1+\lambda_1\right)\alpha_1}\left(u'\right)^2$$

$$+\frac{M^2Ec\Pr}{\alpha_1}(u)^2+\frac{L\alpha_2}{\alpha_1^2}\left(\phi'\right)^2+\frac{L}{\alpha_1}\left(\theta'\phi'\right) \qquad \dots (28)$$

where, $NG=\dfrac{SGT_0^2h^2}{K_f\left(T_1-T_0\right)^2}$ is the entropy generation,

$\alpha_1=\dfrac{T_1-T_0}{T_0}$ is the temperature difference, $\alpha_2=\dfrac{C_1-C_0}{C_0}$
is the concentration difference, $L=\dfrac{R_1D\left(C_1-C_0\right)}{K_f}$ is

diffusion parameter.

On account of Eq. (9), NG can be expressed as

$$NG(y)=NG_0(y)+\varepsilon NG_1(y)e^{it}, \qquad \dots (29)$$

now by substituting the Eqs. (15)-(17) and (29) into the Eq. (28), and likening the coefficient
of like power of ε, we get

$$NG_0=\left(1+\frac{4Rd}{3}\right)\left(\theta_0'\right)^2+\frac{Ec\Pr}{\left(1+\lambda_1\right)\alpha_1}\left(u_0'\right)^2$$

$$+\frac{M^2Ec\Pr}{\alpha_1}(u_0)^2+\frac{L\alpha_2}{\alpha_1^2}\left(\phi_0'\right)^2+\frac{L}{\alpha_1}\left(\theta_0'\phi_0'\right) \qquad \dots (30)$$

$$NG_1 = \left(1 + \frac{4Rd}{3}\right) 2\theta_0' \theta_1'$$

$$+ \frac{Ec\,Pr}{(1+\lambda_1)\alpha_1} 2u_0' u_1' + \frac{M^2 Ec\,Pr}{\alpha_1} 2u_0 u_1$$

$$+ \frac{L\alpha_2}{\alpha_1^2} 2\phi_0' \phi_1' + \frac{L}{\alpha_1}\left(\theta_0'\phi_1' + \theta_1'\phi_0'\right). \qquad \ldots (31)$$

Table 1 — Comparison of the present study with the results provided by NDSolve of θ' at bottom wall, when $H = 1$, $R = 0.5$, $M = 1$, $Rd = 1$, $Pr = 21$, $t = \frac{\pi}{4}$, $Le = 1$, $K_1 = 0.001$, $Nb = Nt = 0.1$, $Q = 0.5$, $\delta = 0.1$, $\lambda = 1$, $\lambda_1 = 1$, and $\gamma = 0.2$.

Parameter	Values	$\theta'_{y=0}$	
		Present scheme	NDSolve
	0.5	0.422554	0.422552
M	1.0	0.384218	0.384217
	1.5	0.340227	0.340226
	2.0	0.301454	0.301453
	0.2	0.249725	0.249732
Ec	0.4	0.338965	0.338963
	0.6	0.429909	0.429908
	0.8	0.522649	0.522648
	0.5	0.273563	0.273563
Rd	1.0	0.384218	0.384217
	1.5	0.496128	0.496127
	2.0	0.581812	0.581811

Bejan number is defined as

Bejan number $(Be) =$

$$\frac{Entropy\ generation\ due\ to\ heat\ and\ Mass\ transfer}{Total\ entropy\ generation}$$

$$Be = \frac{\left(1+\frac{4Rd}{3}\right)(\theta')^2 + \frac{L\alpha_2}{\alpha_1^2}(\phi')^2 + \frac{L}{\alpha_1}(\theta'\phi')}{\left(1+\frac{4Rd}{3}\right)(\theta')^2 + \frac{Ec\,Pr}{(1+\lambda_1)\alpha_1}(u')^2 + \frac{M^2 Ec\,Pr}{\alpha_1}(u)^2 + \frac{L\alpha_2}{\alpha_1^2}(\phi')^2 + \frac{L}{\alpha_1}(\theta'\phi')}. \qquad \ldots (32)$$

The comparative result verifies that there is an excellent agreement between the results provided by NDSolve utilizing MATHEMATICA and the present results which is given in Table 1

3. Results and Discussion

The objective of the present section deals with the influence of pertinent parameters on the velocity, temperature, nanoparticles concentration, entropy generation, and Bejan number profiles of Jeffrey nanoliquid with the help of pictographic results that are revealed in Figs. 2-9. In this study u_s, u_t, θ_s, θ_t,
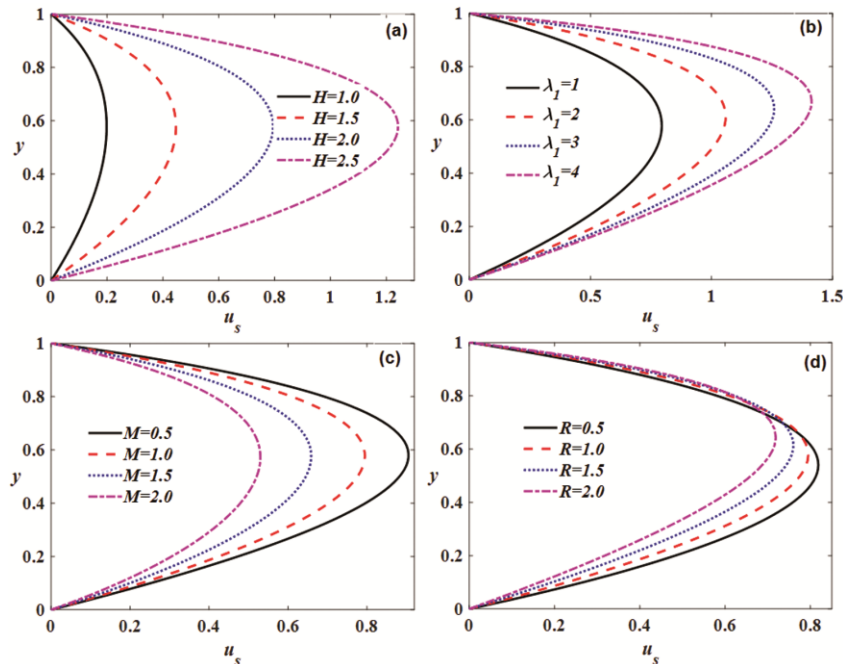

Fig. 2 — Steady velocity profile (a) impression of $H = 1.0, 1.5, 2.0, 2.5$, (b) impression of $\lambda_1 = 1, 2, 3, 4$, (c) impression of $M = 0.5, 1.0, 1.5, 2.0$, and (d) impression of $R = 0.5, 1.0, 1.5, 2.0$.

ϕ_s, ϕ_t denote the steady velocity, unsteady velocity, steady temperature, unsteady temperature, steady concentration and unsteady concentration respectively. Throughout the study, the values of pertinent parameters are respectively fixed as $\text{Pr} = 21$, $M = 1$, $\lambda = \lambda_1 = 1$, $H = 2$, $Ec = 0.5$, $Nb = 0.2$, $t = \dfrac{\pi}{3}$, $Nt = 0.2$, $Le = 1$, $K_1 = 0.001$, $R = 1$, $Q = 0.5$, $\delta = 1$, $\gamma = 1$, unless otherwise stated. Figs. 2(a)-2(d) elucidate the influences of frequency parameter (H), material parameter (λ_1), Hartmann number (M), and cross flow Reynolds number (R) on u_s. Fig. 2(a) displays that the steady

velocity increases as the frequency parameter is increased because a higher frequency amplifies the steady velocity. The same nature can be seen by varying material parameter λ_1 (see Fig. 2(b)). Fig. 2(c) illustrates that the increment in M lowers the steady velocity. This is because the applied magnetic field creates retarding forces (also known as Lorentz forces), which act as resistive drag forces in the reverse direction of the flow. fig. 2(d) illustrates that a rise in R upsurges the velocity near the top wall (suction wall) while it slows the fluid movement near the bottom wall (injection wall).

Figs. 3(a)-3(e) deliberate the impacts of material parameters (λ, λ_1), Hartmann number (M), cross-
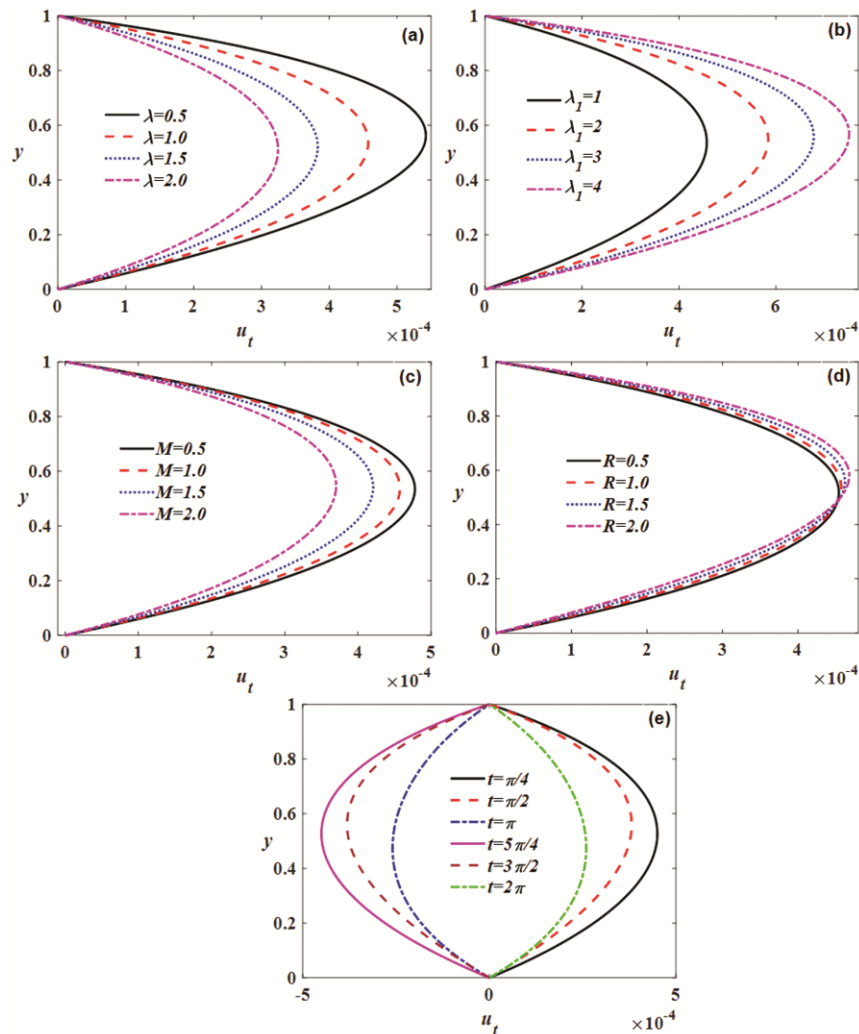

Fig. 3 — Unsteady velocity profile (a) impression of $\lambda = 0.5, 1.0, 1.5, 2.0$, (b) impression of $\lambda_1 = 1, 2, 3, 4$, (d) impression of $M = 0.5, 1.0, 1.5, 2.0$, (d) impression of $R = 0.5, 1.0, 1.5, 2.0$, and (e) impression of $t = \dfrac{\pi}{4}, \dfrac{\pi}{2}, \pi, \dfrac{5\pi}{4}, \dfrac{3\pi}{2}, 2\pi$.
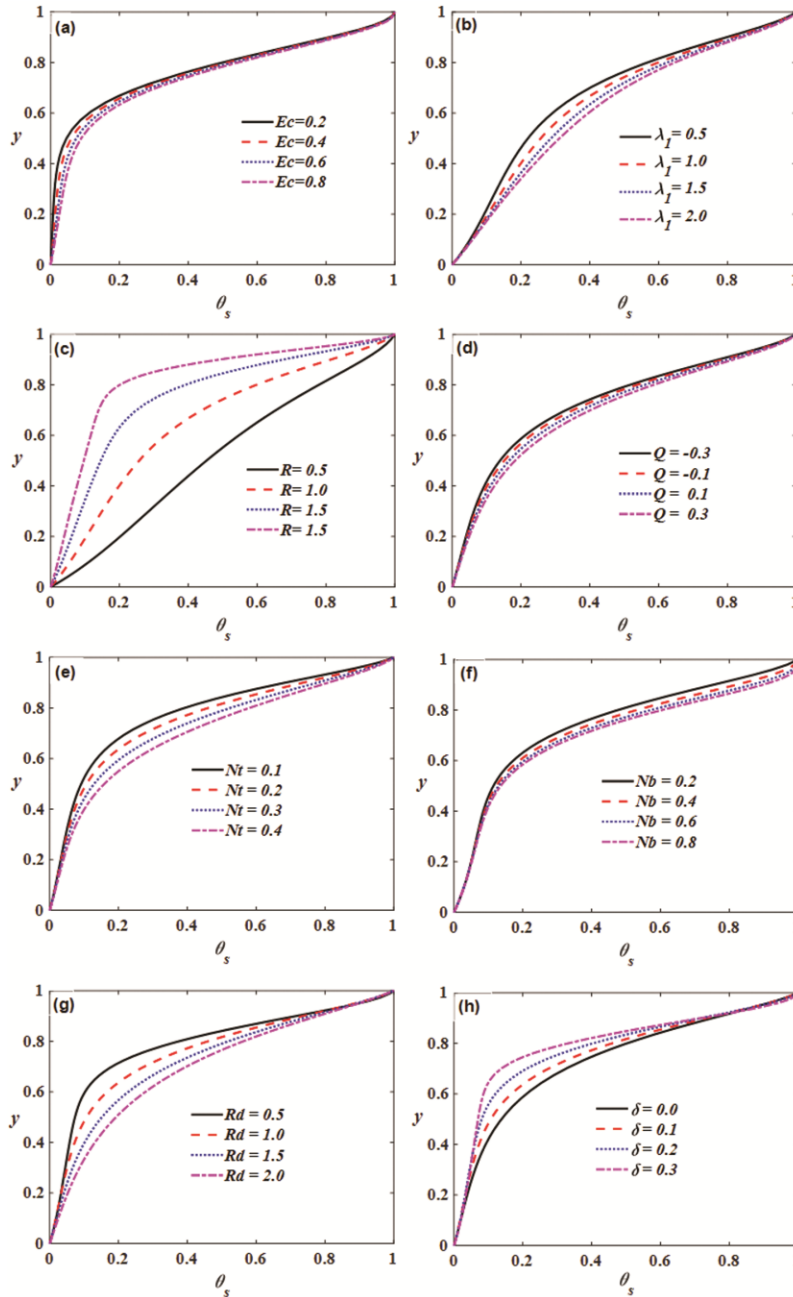
Fig. 4 — Steady temperature profile when $H = 1.5$ (a) impression of $Ec = 0.2, 0.4, 0.6, 0.8$, (b) impression of $\lambda_1 = 0.5, 1.0, 1.5, 2.0$, (c) impression of $R = 0.5, 1.0, 1.5, 2.0$, (d) impressions of $Q = -0.3, -0.1, 0.1, 0.3$, (e) impression of $Nt = 0.1, 0.2, 0.3, 0.4$, (f) impression of $Nb = 0.2, 0.4, 0.6, 0.8$, (g) impression of $Rd = 0.5, 1.0, 1.5, 2.0$, and (h) impression of $\delta = 0.0, 0.1, 0.2, 0.3$.

flow Reynolds number (R), and time (t) on u_t. Fig. 3(a) gives the impact of λ on unsteady velocity. It illustrates that there is a decrease in unsteady velocity with a rise in λ. The opposite nature is depicted in Fig. 3(b) by varying λ_1. Fig. 3(c).

elucidates that the enhancement in Hartman number diminishes the unsteady velocity because the Lorentz forces, which act normal to the flow direction and decreases the velocity of the fluid. Fig. 3(d) portrays that intensifying R expedites the velocity near the top wall (suction wall) while it slows the movement
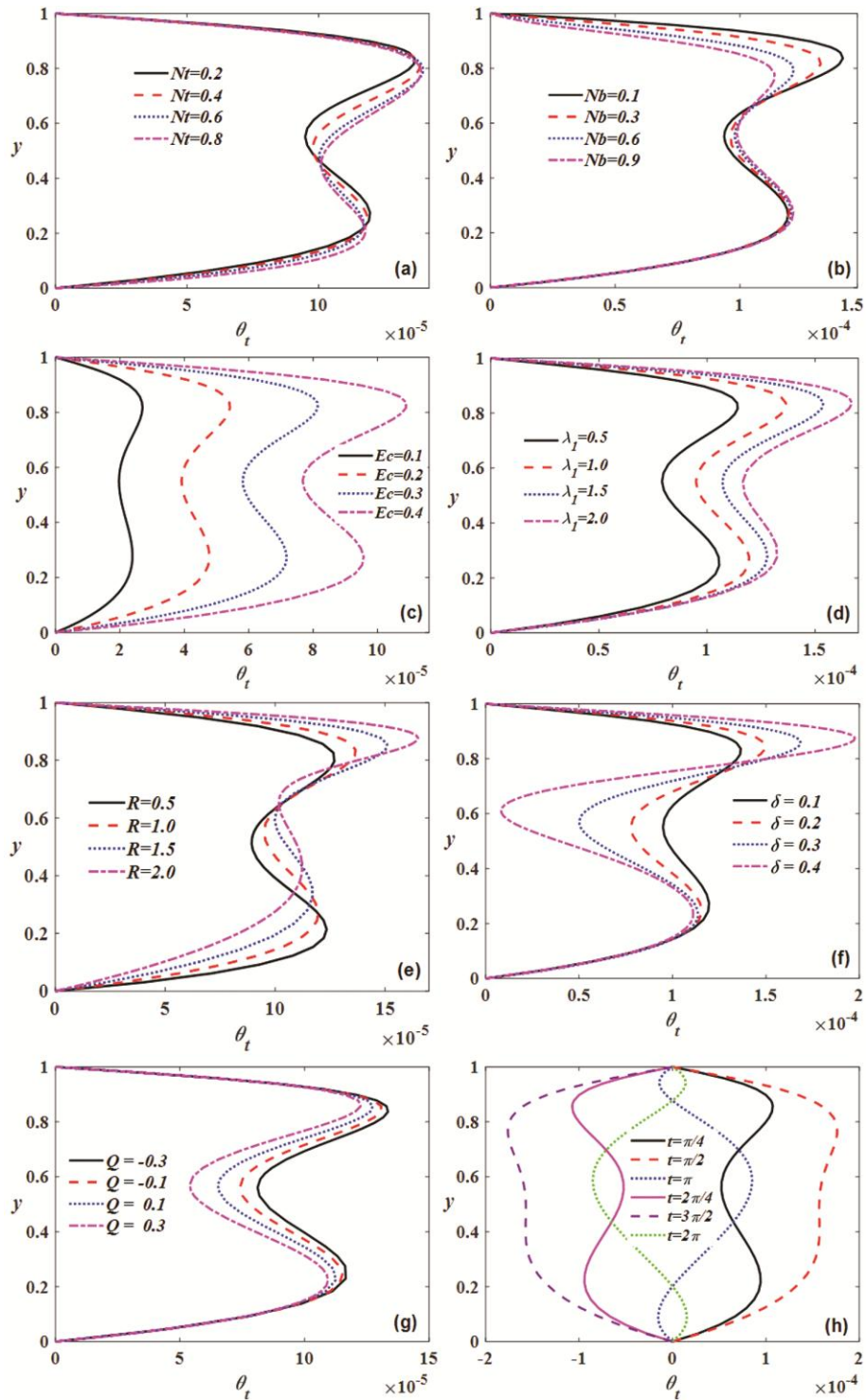
Fig. 5 — Unsteady temperature profile when $H = 2$ (a) impression of $Nt = 0.2, 0.4, 0.6, 0.8$, (b) impression of $Nb = 0.1, 0.3, 0.6, 0.9$, (c) impression of $Ec = 0.1, 0.2, 0.3, 0.4$, (d) impression of $\lambda_1 = 0.5, 1.0, 1.5, 2.0$, (e) impression of $R = 0.5, 1.0, 1.5, 2.0$, (f) impression of $\delta = 0.1, 0.2, 0.3, 0.4$, (g) impressions of $Q = -0.3, -0.1, 0.1, 0.3$, (h) impressions of $t = \dfrac{\pi}{4}, \dfrac{\pi}{2}, \pi, \dfrac{5\pi}{4}, \dfrac{3\pi}{2}, 2\pi$.

of the fluid near the bottom wall (injection wall). From Fig. 3(e) demonstrates that the unsteady temperature is wavering for different values of time (t).

Figs. 4(a)-4(h) present the influences of Ec, λ_1, R, Q, Nt, Nb, Rd and δ on θ_s. Fig. 4(a) demonstrates that the temperature grows with a increment in Ec. Because the Eckert number is linked to frictional forces. As a result, at higher values of Ec, friction occurs inside the fluid which converts

the mechanical energy to thermal energy, therefore the temperature of the nanofluid is upsurged. The same behaviour is observed from Fig. 4(b) by varying λ_1. Fig. 4(c) depicts the impact of R on steady temperature distribution. It demonstrates that the temperature dwindles for the higher values of R. Fig. 4(d) illustrates that the increment in heat sink decreases the temperature whereas the reverse trend can be noticed in temperature for the increment in heat source. Fig. 4(e) shows that an upturn in the thermophoresis parameter raises the nanofluid
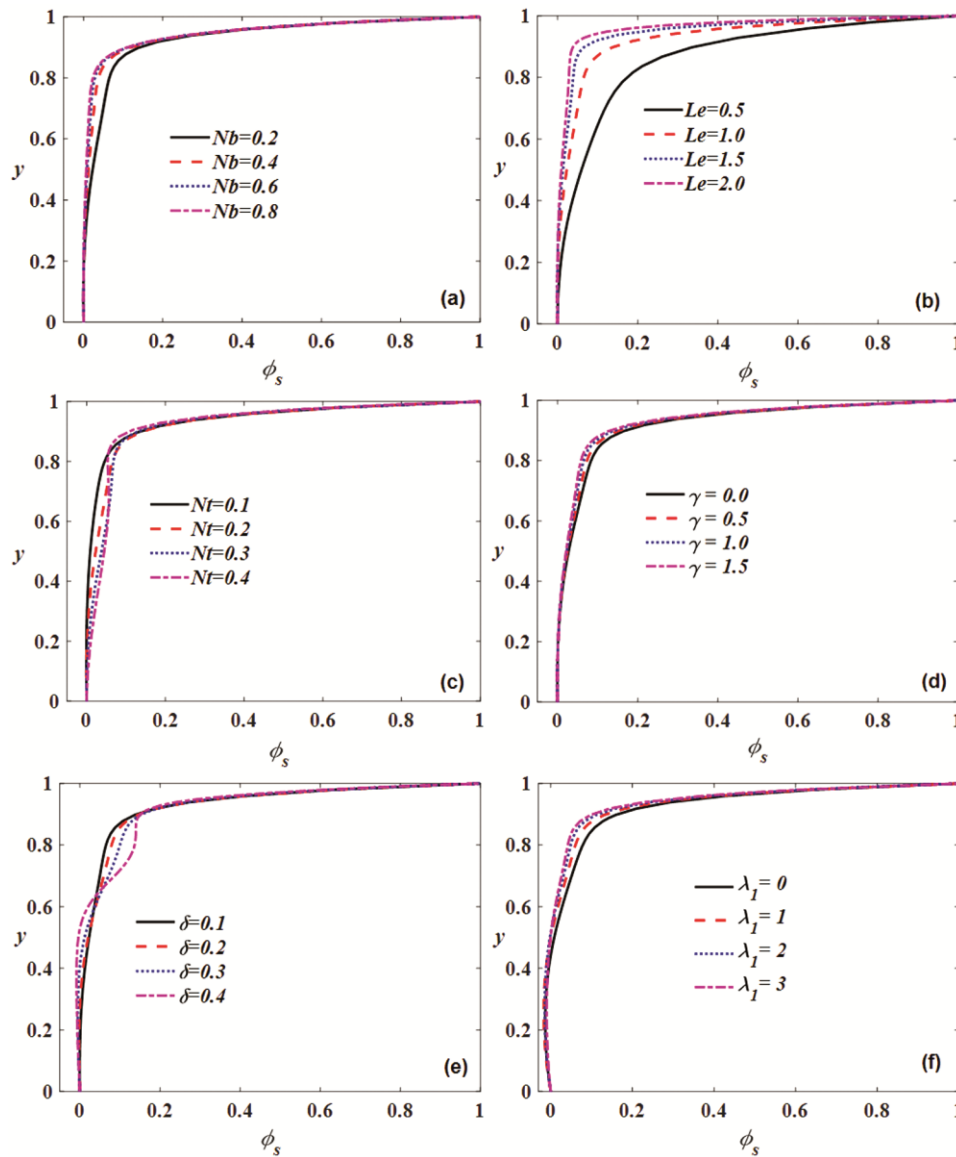

Fig. 6 — Steady concentration profile when $H = 1.5$ (a) impression of $Nb = 0.2, 0.4, 0.6, 0.8$, (b) impression of $Le = 0.5, 1.0, 1.5, 2.0$, (c) impression of $Nt = 0.1, 0.2, 0.3, 0.4$, (d) impression of $\gamma = 0.0, 0.5, 1.0, 1.5$, and (e) impression of $\delta = 0.1, 0.2, 0.3, 0.4$ and (f) impression of $\lambda_1 = 0, 1, 2, 3$.
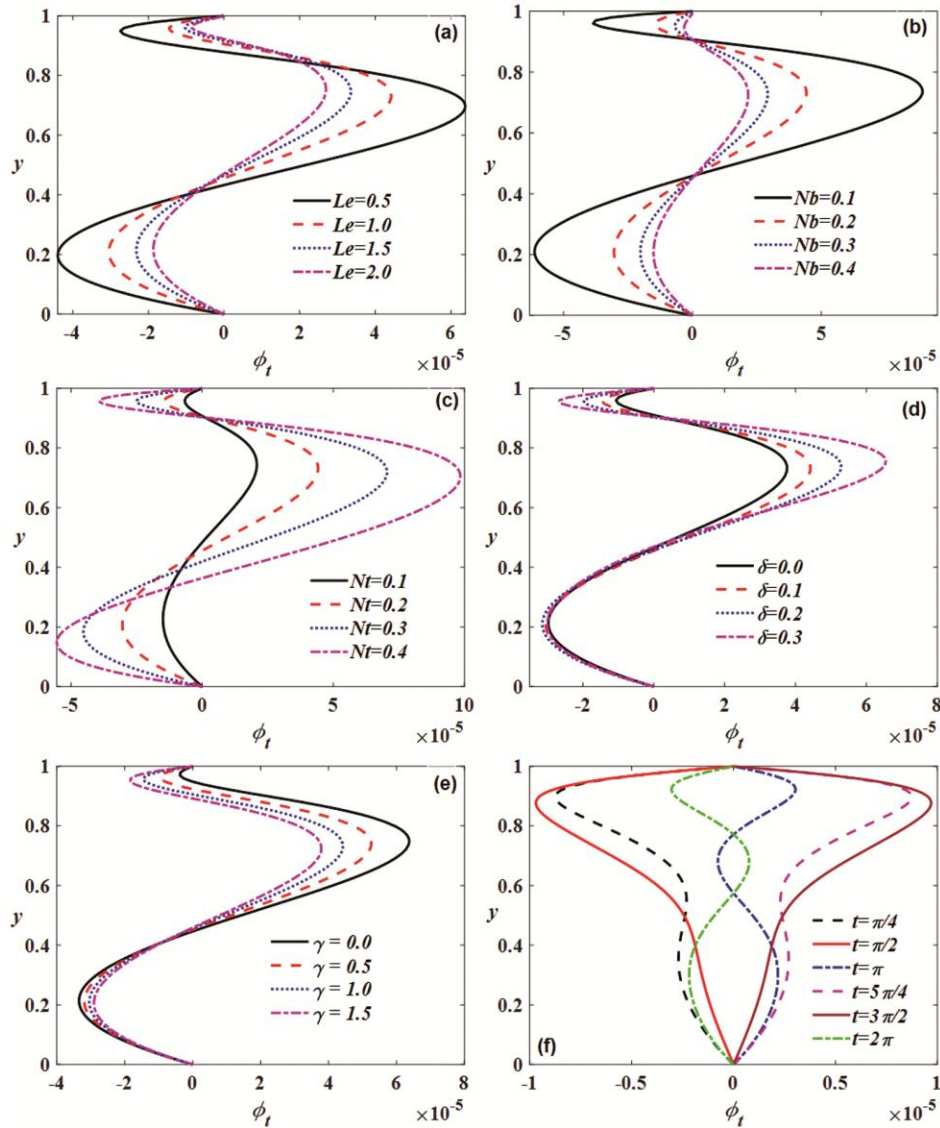
Fig. 7 — Unsteady concentration profile when $H = 1$ (a) impression of $Le = 0.5.1.0, 1.5, 2.0$, (b) impression of $Nb = 0.1, 0.2, 0.3, 0.4$, (c) impression of $Nt = 0.1, 0.2, 0.3, 0.4$, (d) impression of $\delta = 0.0, 0.1, 0.2, 0.3$, (e) impression of $\gamma = 0.0, 0.5, 1.0, 1.5$, and (f) impression of $t = \dfrac{\pi}{4}, \dfrac{\pi}{2}, \pi, \dfrac{5\pi}{4}, \dfrac{3\pi}{2}, 2\pi$.

temperature. Because it tends to shift nanoparticles away from the hot edge towards the cold zone. So, the thickness of the boundary layer and the temperature of the nanofluid are raised. The similar behaviour is noticed by varying Nb (see Fig. 4(f)). Fig. 4(g) presents the steady temperature is declining for the intensifying values of Rd. This drop could be the fact that raising Rd reduces the thickness of the thermal boundary layer. The reverse nature is observed by varying thermal relaxation time parameter (see Fig. 4. (h)).

Figs. 5(a)-5(h) exhibit the influences of Nt, Nb, Ec, λ_1, R, δ, Q, and t on θ_t. Fig. 5(a) and fig. 5(b) portrays that the unsteady temperature is increasing and oscillating with an enhancement of the thermophoretic and Brownian movements. Fig. 5(c) demonstrates that unsteady temperature is ascending with an enhancement of Eckert number (Ec) and also it displays that θ_t profiles show the wavering character. The same behaviour can be seen by varying material parameter (λ_1) (see fig. 5(d)). Fig. 5(e)
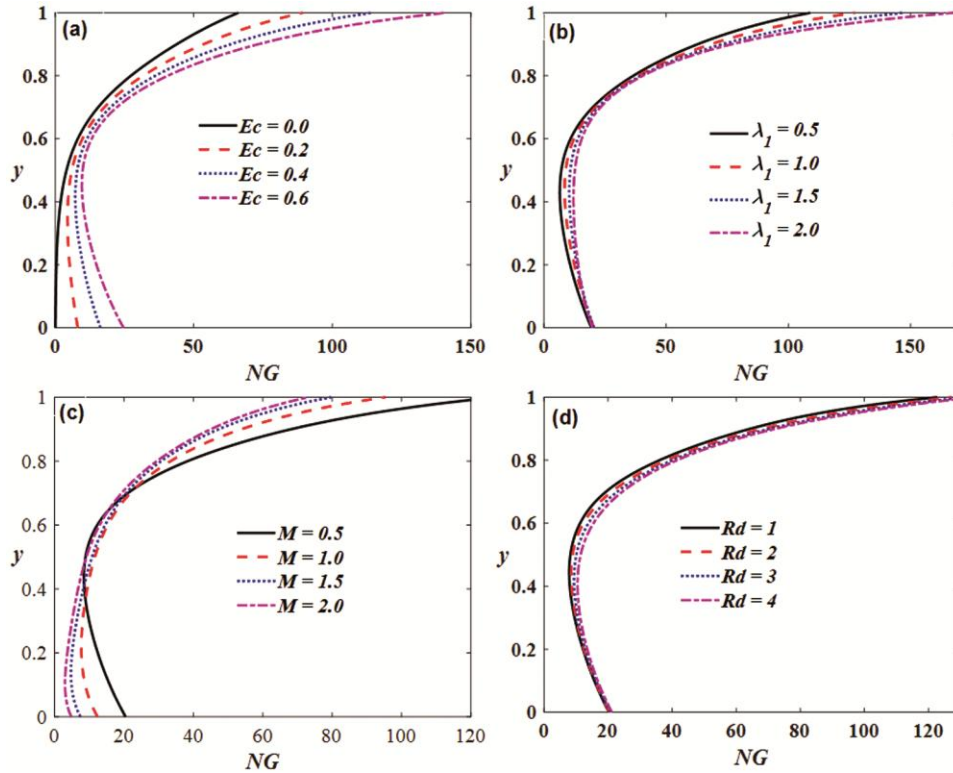
Fig. 8 — Entropy generation profile when $H = 1.5$ (a) impression of $Ec = 0.0, 0.2, 0.4, 0.6$, (b) impression of $\lambda_1 = 0.5, 1.0, 1.5, 2.0$, (c) impression of $M = 0.5, 1.0, 1.5, 2.0$, (d) impression of $Rd = 1, 2, 3, 4$.
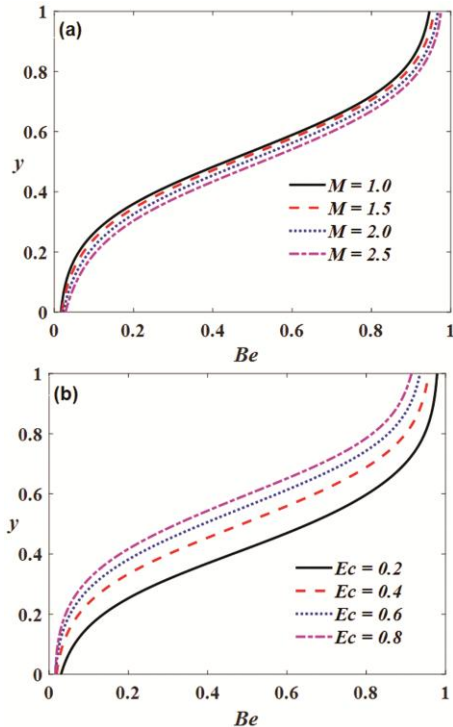

Fig. 9 — Bejan number profile when $H = 1$ (a) impression of $M = 1.0, 1.5, 2.0, 2.5$, (b) impression of $Ec = 0.2, 0.4, 0.6, 0.8$.

establishes the impact of R on θ_t. There is an oscillatory tendency in θ_t profile depicted in this figure for high values of R. Fig. 5(f) shows that θ_t profile oscillates as the thermal relaxation time parameter is raised. The same nature is noticed by varying the values of the heat source (Q > 0) and heat sink (Q < 0) (see Figs. 5(g)). Fig. 5(h) demonstrates that the unsteady temperature is wavering for different values of time (t).

Figs. 6(a)-6(f) exhibit the effects of Nb, Le, Nt, γ, δ, and λ_1 on steady concentration nanoparticles distribution (ϕ_s). Fig. 6(a) illustrates that the steady concentration decreases for large Nb. Physically, collisions and abrupt movement of nanoparticles usually happen for higher values of Nb and thus more heat releases. As a result, steady concentration decreases. The same nature is observed by varying Lewis number (Le) on steady concentration distribution. Fig. 6(c) demonstrates that the steady concentration rises with an increment in Nt. Because the temperature gradient is intimately related to

thermophoresis, then the temperature of the fluid rises as the (Nt) increases, and therefore the concentration rises. The reverse behavior is noticed by varying chemical reaction parameter (γ) (see Fig. 6(d)). Fig. 6(e) shows that the influence of δ on steady concentration nanoparticles. It is clearly observed that the steady concentration of nanoparticle declines with a rise in thermal relaxation property (δ). The opposite nature is observed by varying material parameter (λ_1) (see Fig.6(f)).

Figs. 7(a)-7(f) exhibit the impacts of Le, Nb, Nt, δ, γ and t on ϕ_t. Figs. 7(a) and 7(b) demonstrates that the unsteady nanoparticles concentration profile displays increasing near the walls and oscillating at the centre of the walls as the increment of Le and Nb. Fig. 7(c) and 7(d) illustrates that the concentration of unsteady nanoparticles declining near the walls and oscillates at the center of the walls with increasing thermophoresis (Nt) and thermal relaxation time (δ). Fig. 7(e) presents that the nanoparticles concentration is increased in a bottom wall while it is decreased in the top wall for higher values of γ. Fig. 7(f) displays the impact of time (t) on ϕ_t. It shows that the oscillating character for different values of time (t).

Figs 8(a)-8(d) indicate the impacts of Eckert number, material parameter, Hartmann number, and

radiation parameter on entropy generation (NG) profiles. Fig 8(a) demonstrates that the entropy generation is upsurged for higher values of Ec due to the kinetic energy dominates the enthalpy difference at large Eckert numbers. As a result, the entropy generation is increased. A similar nature is observed by varying material parameter (see Fig. 8(b)). Fig 8(c) presents that the entropy generation is reduced for higher values of M. Due to the retarding forces created by the applied magnetic field, which decrease the thermal boundary layer. Fig 8(d) demonstrates that the influence of thermal radiation parameter on entropy generation (NG). It can be seen that entropy number upsurges with the rise in Rd, because of thermal radiation's relative commitment to conductive heat.

Figs 9(a)-9(b) elucidate the influences of H and Ec on Bejan number of Jeffrey nanofluid. Fig. 9(a) displays the Bejan number is accelerated due to intensifying the values of M because more resistance acts on fluid flow. The reverse trend is noticed by varying Eckert number (see fig. 9(b)). The Nusselt and Sherwood number distribution for steady and unsteady influences (Nu_s, Nu_t, Sh_s, Sh_t) at the bottom wall for various values of Ec, Nb, Nt, Rd, and R are presented in Table 2. It indicates that Nu_s and Nu_t at the bottom wall are enhanced while increasing, Eckert number, Brownian motion,

Table 2 — Variations of heat and mass transfer rate at the bottom wall for steady and unsteady effects (Nu_s, Nu_t, Sh_s, Sh_t) for various values of λ_1, Ec, Nb, Nt, Rd, R at $H=2$, $M=1$, $\lambda=\lambda_1=1$, $Ec=0.5$, $\Pr=21$, $t=\dfrac{\pi}{3}$, $Nb=0.2$, $Nt=0.2$, $Le=1$, $K_1=0.001$, $R=1$, $Q=0.5$, $\delta=1$, $\gamma=1$.

Parameters	Values	$(Nu_s)_{y=0}$	$(Nu_t)_{y=0}$	$(Sh_s)_{y=0}$	$(Sh_t)_{y=0}$
Ec	0.2	1.539849	0.001721	-0.054597	-0.000109
	0.4	3.134793	0.003584	-0.122155	-0.000236
	0.6	4.843793	0.005608	-0.199563	-0.000385
Nb	0.1	3.968939	0.004573	-0.318842	-0.000616
	0.2	3.974077	0.004575	-0.159513	-0.000308
	0.3	3.978640	0.004576	-0.106431	-0.000205
Nt	0.1	3.779939	0.004342	-0.074364	-0.000138
	0.2	3.974077	0.004575	-0.159513	-0.000308
	0.3	4.217373	0.004836	-0.260032	-0.000518
Rd	1.0	3.044523	0.003881	-0.213600	-0.000442
	2.0	3.974077	0.004575	-0.159513	-0.000308
	3.0	4.874265	0.005123	-0.124424	-0.000240
R	0.5	7.448737	0.006282	-0.560066	-0.000717
	1.0	3.974077	0.004575	-0.159513	-0.000308
	1.5	2.249538	0.003230	-0.047529	-0.000114

thermophoresis, and radiation parameter whereas the opposite nature can be seen with the enhancement in cross flow Reynolds number. Also, this table shows that Sh_s and Sh_t at the bottom wall are increased for giving higher values in Nb, R and Rd. Further, it is clearly noticed that Sh_s and Sh_t at the bottom wall are a declining function of Ec, and Nt.

5 Conclusion

The present study deals with the entropy generation on pulsatile flow of Jeffrey nanofluid in a porous channel with Cattaneo-Christov theory. Buongiorno nanofluid model is focused to view the Brownian movement and thermophoretic influences. The effects of thermal radiation, Ohmic heating, and heat source/sink are considered. The governing equations are transformed to a system of ordinary differential equations by applying the perturbation procedure then numerically tackled with fourth-order Runge-Kutta scheme aided by shooting technique. The impact of various pertinent parameters and variables on velocity, temperature, nanoparticles concentration, entropy generation, and Bejan number are presented graphically. Distributions of Nu and Sh are tabulated for different values of physical parameters are discussed in detail. The main outcomes are

- The temperatures are rising functions by mounting the Ec, Nb, and Nt.
- The concentration of the nanoparticles is declining with an increment of chemical reaction, Lewis number, and Brownian motion.
- The Nusselt number is magnifying for higher values of Nb and Ec whereas the opposite nature can be identified with an increment in R and Rd at the bottom wall.
- Mass transfer rate is a decreasing function of Ec and Nt.
- The entropy generation is increasing for intensifying Ec, λ_1, and Rd whereas the reverse trend can be noticed with an enhancement in M.
- Bejan number is dwindling for escalating Hartmann number whereas it is increasing with the enhancement in viscous dissipation.

References
1 Javed M, Imran N & Rao A I, *Heat Trans*, 50 (2021) 6358.
2 Padma R, Tamil Selvi R & Ponalagusamy R, *J Phys Conf Ser*, 1850 (2021) 012039.
3 Adesanya S O, Falade J A & Makinde O D, *UPBSciBull, Ser D,* 77 (2015) 25..
4 Wang C, *ASME J Appl Mech*, 38 (1971) 553.
5 Radhakrishnamacharya G & Maiti M K, *Int J Heat Mass Trans*, 20 (1977) 171.
6 Rajamani S, Reddy A S, Srinivas S & Ramamohan T R, *Indian J Pure Appl Phys,* 60 (2022) 354.
7 Wang X, Qiao Y, Qi H & Xu H, *Int Commun Heat Mass Trans*, 133 (2022) 105930.
8 Ali A, Fatima A, Bukhari Z, Farooq H & Abbas Z, *Korea Aust Rheol J*, 33 (2021) 79.
9 Sadeghi M R, Jahangiri M & Saghafian M, *J Brazilian Soc Mech Sci Eng*, 42 (2020) 1.
10 Selvi R T, Ponalagusamy R & Padma R, *Int J Appl Comput Math*, 7 (2021) 1.
11 Shit G C, Maiti S, Roy M & Misra J C, *Math Comput Simul*, 166 (2019) 432.
12 Govindarajulu K & Reddy A S, *Phys Fluids*, 34 (2022) 013105.
13 Mabood F, Imtiaz M & Hayat T, *Heat Trans*, 49 (2020) 2706.
14 Sulochana C, Ashwinkumar G P & Sandeep N, *Alexandria Eng J*, 55 (2016) 1151.
15 Raza J, Mebarek-Oudina F, Ram P & Sharma S, *Defect Diffus Forum*, 401 (2020) 92.
16 Venkatesan G & Reddy A S, *Indian J Pure Appl Phys*, 60 (2022) 437.
17 Li Y X, Alshbool M H, Lv Y P, Khan I, Khan R M & Issakhov A, *Case Stud Therm Eng*, 26 (2021) 100975.
18 Khan S A, Hayat T & Alsaedi A, *Chin J Phys*, 76 (2022) 205.
19 Saif RS, Muhammad T, Sadia H & Ellahi R, *Phys A Stat Mech Appl*, 551 (2020) 124060.
20 Hayat T, Javed M, Imtiaz M & Alsaedi A, *Results Phys*, 8 (2018) 341.
21 Chu Y M, Khan M I, Khan N B, Kadryl S, Khan S U, Tlili I & Nayak M K, *Int Commun Heat Mass Trans*, 118 (2020) 104893.
22 Khan M I, Hayat T, Waqas M, Alsaedi A & Khan M I, *J Hydrodyn*, 31 (2019) 42.
23 Hussain Z, Hussain A, Anwar M S & Farooq M, *J Therm Anal Calorim*, 147 (2022) 3391.
24 Hayat T, Ullah H, Ahmad B & Alhodaly M S, *Int Commun Heat Mass Trans*, 120 (2021) 104965.
25 Aldabesh A, Hussain M, Khan N, Riahi A, Khan S U & Tlili I, *Case Stud Therm Eng*, 23 (2021) 100820.
26 Rajkumar D & Reddy A S, *Phys Scr*, 96 (2021) 125233.
27 Buongiorno J, *J Heat Trans,* 128 (2006) 128.
28 Choi S U S & Eastman J, *Am Soc Mech Eng Fluids Eng Div*, 231 (1995) 99.
29 Abbasi F M, Shehzad S A, Hayat T & Alhuthali M S, *J Hydrodyn*, 28 (2016) 840.
30 Su X, *Indian J Pure Appl Phys*, 55 (2017) 564.
31 Dogonchi A S & Ganji D D, *J Taiwan Inst Chem Eng*, 80 (2017) 52.
32 Abbas S Z, Wang X, Khan W A, Hobiny A & Iqbal K, *J Energy Storage*, 51 (2022) 104462.

33 Hayat T, Shah F & Alseadi A, *Int Commun Heat Mass Trans*, 119 (2020) 104824.

34 Dogonchi A S, Chamkha A J, Seyyedi S M & Ganji D D, *Heat Trans Asian Res*, 47 (2018) 735.

35 Hamid M, Usman M, Khan Z H, Haq R U & Wang W, *Eur Phys J Plus*, 133 (2018) 527.

36 Mondal P & Mahapatra T R, *Int J Mech Sci*, 208 (2021) 106665.

37 Salawu S O & Ogunseye H A, *Results Eng*, 5 (2020) 100072.

38 Basha H T & Sivaraj R, *Proc Inst Mech Eng Part E J Process Mech Eng*, 235 (2021) 1575.

39 Falade J A, Adesanya S O, Ukaegbu J C & Osinowo M O, *Alexandria Eng J*, 55 (2016) 69.

40 Usman, Ghaffari A, Mustafa I, Muhammad T & Altaf Y, *Case Stud Therm Eng*, 28 (2021) 101370.

41 Hayat T, Kanwal M, Qayyum S & Alsaedi A, *Phys A Stat Mech Appl*, 544 (2020) 123437.

42 Almakki M, Nandy S K, Mondal S, Sibanda P & Sibanda D, *Heat Trans Asian Res*, 48 (2019) 24.

43 Javed M F, Waqas M, Khan M I, Khan N B, Muhammad R, Rehman M U, Khan S W & Hassan M T, *Appl Nanosci*, 10 (2020) 3011.

44 Pal D, Mondal S & Mondal H, *Int J Ambient Energy*, 42 (2021) 1712.

45 Rehman S U, Haq R U, Khan Z H & Lee C, *J Taiwan Inst Chem Eng*, 63 (2016) 226.